Global Journal of Engineering and Technology Advances
eISSN: 2582-5003
Cross Ref DOI: 10.30574/gjeta
Journal homepage: https://gjeta.com/

(REVIEW ARTICLE)

Check for updates

Effects of interfacial defects of the p-CuO/n-TiO2 on the CuO/CdS/TiO2 solar cell performance

Gulsan. T. Kamal *, Nadim. K. Hassan, Abdulrahman. R. Hammood and Abdul Kareem Dahash Ali

Department of physics, College of Education for pure science, University of Tikrit.

Global Journal of Engineering and Technology Advances, 2024, 18(03), 082–089

Publication history: Received on 27 January 2024; revised on 09 March 2024; accepted on 12 March 2024

Article DOI: https://doi.org/10.30574/gjeta.2024.18.3.0039

Abstract

Due to its high absorption of solar energy and low heat emission, copper oxide has been used in a growing number of recent investigations. The crystal structure of CuO is monoclinic at 99.54°. There are four oxygen atoms firmly bonded to each copper atom. The results show a decrease in V_{oc}, Jsc, and η with increasing interfacial defect density, where Voc decreases from 0.652 V at a defect density of $10^{10}cm^{-2}$ to 0.648 V at a defect density of $10^{14}cm^{-2}$, Jsc decreases from 18.31 mA/cm2 at a defect density of $10^{10}cm^{-2}$ to 13.20. mA/cm2 at the efficiency defect density of $10^{14}cm^{-2}$, F.F increases from 37.69% at the defect density of $10^{10}cm^{-2}$ to 46.87% at the defect density of $10^{14}cm^{-2}$, η decreases from 4.51% at the defect density of $10^{10}cm^{-2}$ to 4.01% at the defect density of $10^{14}cm^{-2}$ As the cross-section of carrier capture increases, the length of propagation will decrease, and thus the durability of the carriers will decrease. The results, are a decrease in Voc with an increase in the cross-section ranges from 0.791 V to 0.776 V, Jsc from 27.69 (mA/cm2) to 20.60 (mA/cm2), F.F from 84.59% to 70.21%, and η from 18.53% to 11.24%.

Keywords: Interfacial defects; CuO; TiO_2; Solar cell; SCAPS-1D; Energy level; Carrier trapping

1. Introduction

A multitude of photoactive absorber materials have been used recently to produce a wide range of photovoltaic (PV) systems. Since silicon solar cells account for more than 90% of the worldwide solar market, they are the most extensively utilized type of solar cells.[1], even though they now operate at more than 26% efficiency[2]. Si-based solar cells are rather expensive, hence many efforts have been made to produce low-cost, high-efficiency solar cells .[3-6]It is expected that a safe and benign material such as TiO_2 would eventually be able to replace silicon-based solar cells. However, the use of TiO_2 as the active material in solar cells is still relatively new, and there are fewer papers on the subject..[7, 8]TiO_2 and CuO based heterojunctions are promising options for solar cell components and photocatalytic applications.. [9-11]. Materials used in P-type solar cells, such as absorber layers Cu_2O or CuO, have low direct band gaps between 2.0 and 2.6 eV.[12]and 1.0–2.1 eV [13], respectively. With a gap energy of over 3 eV, TiO2 is an n-type semiconductor with a wide bandgap that is well-known for its many functions and potential as a material for dye-sensitized solar cells. [14, 15]. TiO2 is regarded as a window layer or buffer material.[12].

2. Cell Structure

The solar cell structure is composed of (TiO2 / CdS / CuO) as shown in Fig (1) Titanium dioxide (Tio_2) is the window layer, which is one of the transparent metal oxides and has a relatively large energy gap of about (3.2 eV). Then, the buffer layer Cadmium Sulfide CdS has a suitable energy gap of (2.4 eV) and works on tuning between the window layer and the absorption layer. Then comes the p-type (CuO) absorption layer, which has an energy gap that ranges from 1.21 to 1.51 eV (1.9eV).

* Corresponding author: Gulsan. T. Kamal

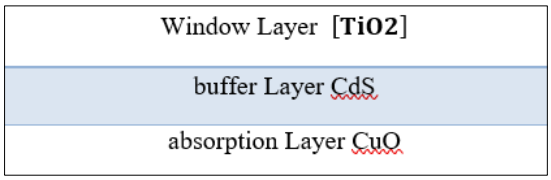

Figure 1 The solar cell structure

Table 1 Materials parameters used in the simulation

Parameters	**Symbol (unit)**	**TiO2**	**CdS [16]**	**CuO**
Thickness	W(μm)	0.3	0.1	Variable
Bandgap	Eg (ev)	3.2	2.4	1.5
Electron affinity	χ (ev)	4.2	4.2	4.070
Dielectric permittivity	ϵr	10	9	18.100
CB effective density of states	N_C (cm^{-3})	2×10^{17}	2.2×10^{18}	2.2×10^{19}
VB effective density of states	N_V (cm^{-3})	6×10^{19}	1.8×10^{19}	5.5×10^{20}
Electron thermal velocity	V_n (cm/s)	1.0×10^{7}	1.0×10^{7}	1.0×10^{7}
Hole thermal velocity	V_P (cm/s)	1.0×10^{7}	1.0×10^{7}	1.0×10^{7}
Electron mobility	μ_n (cm^2/v. s)	100	100	100
Hole mobility	μ_p (cm^2/v. s)	25	25	0.1
Shallow uniform donor density	ND (1/cm3)	1×10^{17}	1×10^{21}	0
Shallow uniform acceptor density	NA (1/cm3)	0	0	Variable

3. Numerical simulation in SCAPS-1D

A one-dimensional solar cell modeling tool called SCAPS-1D was developed at the Department of Electronics and Information Systems (EIS), University of Gent, Belgium, and was used to numerically study the solar cell. Up to seven layers can be added to the software's cell definition panel to increase its suitability for simulating solar cells. Physical properties include bandgap, electron affinity, and dielectric permittivity, among others. [17]. The software's main role is the solution of semiconductor equations. We begin by writing a Poisson equation..[18].

$$-\frac{d^2\psi}{dx^2} = \frac{dE}{dx} = \frac{q}{\varepsilon_s}[\mathbf{p} + \boldsymbol{n} + \boldsymbol{N_D^+} - \boldsymbol{N_A^-}] \quad \text{..... [1]}$$

where the concentration of donors is represented by N_D and that of acceptors by N_A; P is the hole density, n is the electron density, ψ is the electrostatic potential, E is the electric field, and $\boldsymbol{\varepsilon_s}$ is the relative permittivity.

The continuity equation can be obtained by using the relationship that follows.

$$\frac{\partial n}{\partial t} = \frac{1}{q}\frac{\partial J_n}{\partial x} + \boldsymbol{G_n} - \boldsymbol{R_n} \quad \text{..... [2]}$$

$$\frac{\partial p}{\partial t} = -\frac{1}{q}\frac{\partial J_p}{\partial x} + \boldsymbol{G_p} - \boldsymbol{R_p} \quad \text{..... [3]}$$

where (Gp) is the rate of electron (hole) generation, (R) is the rate of electron (hole) recombination, and Jn (Jp) is the current density of electron (hole) (hole). Solving the Poisson and continuity equations yields the equations for the charge carrier diffusion and drift density.[19].

$$\text{Jn} = \boldsymbol{q}(\boldsymbol{n}\mu_n\boldsymbol{E} + \text{Dn}\frac{\boldsymbol{dn}}{\boldsymbol{dx}}) \quad \text{..... [4]}$$

$$Jp= \boldsymbol{q}(\boldsymbol{n}\mu_{\boldsymbol{p}}\boldsymbol{E} + Dp\frac{\boldsymbol{dp}}{\boldsymbol{dx}}) \text{ ..... [5]}$$

Where q The charge , μn (μp) are the mobility of electron (hole) , (E)electric field, (D) diffusion coefficient .The total current of the solar cell was calculated using the following formulas. [20].

$$\mathbf{I} = \mathbf{I_0}\left(\mathbf{exp}\ \frac{\boldsymbol{qV}}{\boldsymbol{nKT}} - \mathbf{1}\right) - \mathbf{I_L} \text{ ..... [6]}$$

where T is the temperature in Kelvin, K is the Boltzmann constant, and IL is the current of light. To calculate the open circuit voltage (Voc), which is the voltage that occurs when there is no current and is defined by the following equation.

$$\mathbf{V_{OC}} = \frac{\mathbf{KT}}{\mathbf{q}}\ \mathbf{Ln}\left(\frac{\mathbf{I_L}}{\mathbf{I_o}} - \mathbf{1}\right) \approx \frac{\mathbf{KT}}{\mathbf{q}}\ \mathbf{Ln}\left(\frac{\mathbf{I_L}}{\mathbf{I_o}}\right) \text{.....[7]}$$

Where Io is the saturation current, which may be found using the equation below.

$$\mathbf{I_0} = \boldsymbol{A}\left[\frac{\boldsymbol{q}\,\boldsymbol{D_n}\boldsymbol{n_i}^2}{\boldsymbol{L_n}\boldsymbol{N_A}} + \frac{\boldsymbol{q}\,\boldsymbol{D_p}\boldsymbol{n_i}^2}{\boldsymbol{L_p}\boldsymbol{N_D}}\right] \text{ ..... [8]}$$

The length of electron and hole diffusion is represented by the diode's cross-sectional area, which is indicated by Ln and Lp. The relationship between the open circuit voltage and short circuit current is shown in the following relationship.

$$\mathbf{Isc} = \mathbf{I_0}\left(\mathbf{exp}\frac{\mathbf{qvoc}}{\mathbf{kT}} - \mathbf{1}\right) \text{ ..... [9]}$$

where the following equations show the relationships between the variables Voc, Isc, η, and FF.[18].

$$\mathbf{FF} = \frac{\mathbf{V_{max}}\,\mathbf{I_{max}}}{\mathbf{V_{oc}}\,\mathbf{I_{sc}}} \text{ ..... [10]}$$

$$\boldsymbol{\eta} = \frac{\mathbf{P}\boldsymbol{max}}{\mathbf{p_{in}}} \times \mathbf{100}\% \text{.....[11]}$$

$$\boldsymbol{\eta} = \frac{\mathbf{FF}\times\mathbf{I_{sc}}\times\mathbf{V_{oc}}}{\mathbf{p_{in}}} \times \mathbf{100}\% \text{ ..... [12]}$$

The minority carrier lifts time, or the average amount of time needed to recombine minority carriers, must be determined. There is a link between it and the concentrations of doping and recombination. [21]:

$$\boldsymbol{\tau} = \frac{\mathbf{1}}{\boldsymbol{\sigma}\mathbf{V_{th}}\mathbf{N_t}} \text{ ..... [13]}$$

$$\boldsymbol{\tau} = \frac{\boldsymbol{\Delta}\mathbf{n}}{\mathbf{R}} \text{ ..... [14]}$$

where N_t is the concentration of defects, V_{th} is the thermal speed, R is the recombination rate, σ is the capture cross section, and Δn is the concentration of surplus minority carriers.

The mobility of the charge carrier in bulk semiconductor material can have a major effect on a solar cell's performance..[22]. As The minority carrier diffusion length (diffusion length Lm) is largely dependent on mobility. Diffusion length is the average length scale over which a material can diffuse in a semiconductor before recombining. The definition of minority carrier diffusion length is given in Equation 15. [23].

$$\mathbf{L_{diff}} = \sqrt{\mathbf{D}\,\boldsymbol{\tau}} \text{ ..... [15]}$$

where τ is the minority carrier's lifespan and D is the diffusion coefficient. Equation 16 provides the relationship for D.

$$D = \mu\frac{\mathbf{KT}}{\mathbf{q}} \text{ ..... [16]}$$

The carrier's mobility, charge, Boltzmann's constant, and temperature are denoted by the variables μ, q, and T, respectively.

The value of equation 16 will be substituted for equation 15 in that sequence, yielding equation 17.

$$L_{diff} = \sqrt{\mu \frac{KT}{q} \tau} \quad \text{.....[17]}$$

Equation 18 indicates that the mobility of minority carriers will have a major effect on the diffusion length. A solar cell's photocurrent will be improved by increased mobility because it will be more likely for photogenerated charge carriers to aggregate at the terminals. On the other hand, if mobility decreases, solar cell efficiency will also fall.

4. Results and discussion

4.1. Effect of the energy level of interfacial defects of the p-CuO/n-TiO2 cell

In this part, we will study the effect of interfacial defects on the operation of the solar cell with the change in the defect level of the interfacial state in the donor-like state of the equivalence band, at the Gaussian distribution, while the other parameters remain constant without change. In the case of the donor alum, the results can be explained as in Figure (2).

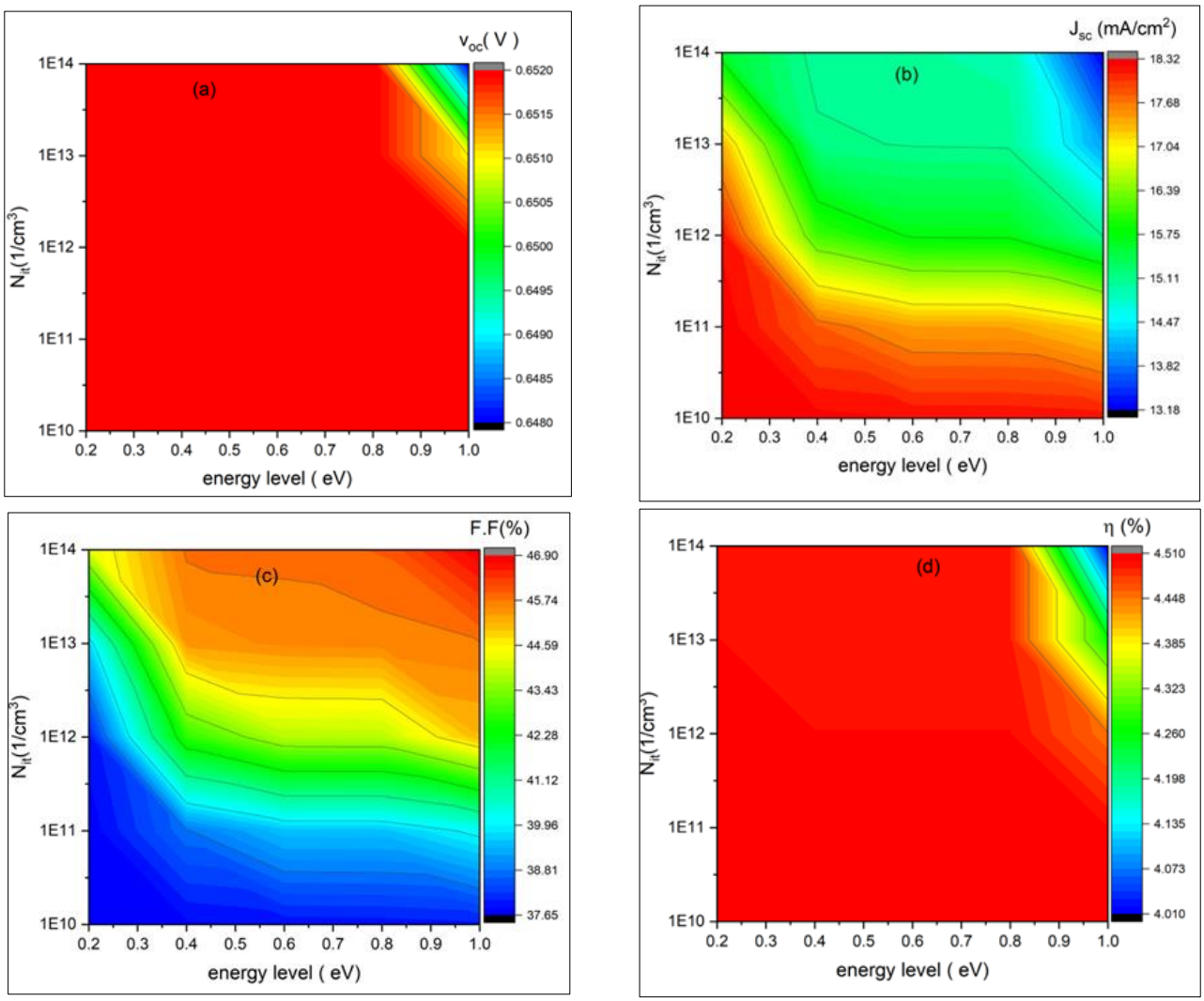

Figure 2 The effect of the level of donor defects and the concentration of interfacial defects on the operation of the solar cell

The results show a decrease in Voc, Jsc, and η with increasing interfacial defect density, where Voc decreases from 0.652 V at a defect density of $10^{10}cm^{-2}$ to 0.648 V at a defect density of $10^{14}cm^{-2}$, Jsc decreases from 18.31 mA/cm2 at a defect density of $10^{10}cm^{-2}$ to 13.20. mA/cm2 at the efficiency defect density of $10^{14}cm^{-2}$, F.F increases from 37.69% at the defect density of $10^{10}cm^{-2}$ to 46.87% at the defect density of $10^{14}cm^{-2}$, η decreases from 4.51% at the defect density of $10^{10}cm^{-2}$ to 4.01% at the defect density of $10^{14}cm^{-2}$. The reason for this decrease is due to an increase in the union rate, which leads to a decrease in quantitative efficiency, as in Figure (3).

In the case of the donor alum, the results show that Voc, Jsc, F.F, and η are not affected by the change in the defect level in the case of the donor alum, because all the interfacial states within this energy range lie below the Fermi level, and this leads to filling these states and transforming them into a neutral state. The reason for all of the above is that the bundle diagram in the case of donor alum is identical to the bundle diagram in the case of neutral (neutral).

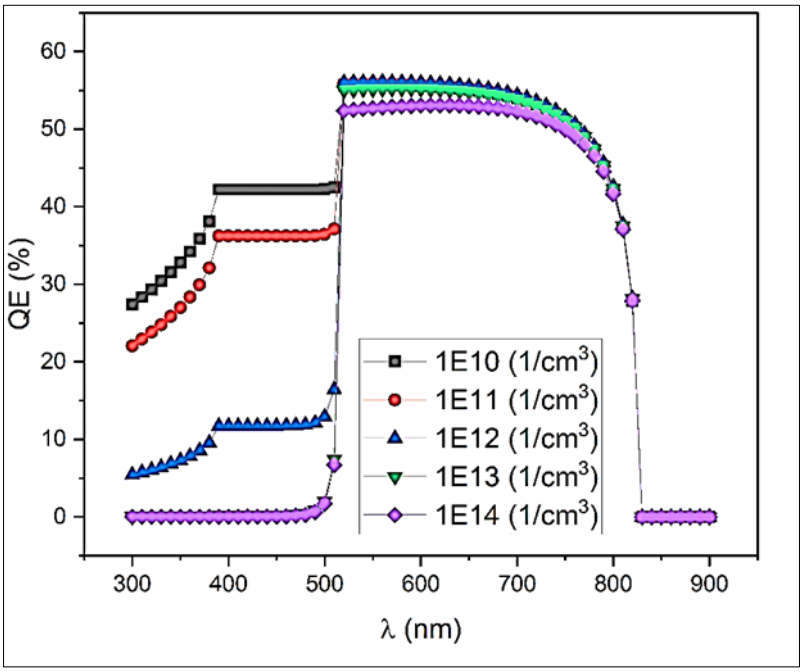

Figure 3 Quantum efficiency with varying interfacial defects

4.2. Effect of interfacial defect concentration and carrier trapping cross section

The carrier capture cross section (Cn, Cp) has a significant impact on the electrical properties of the solar cell because the carrier capture cross section has a relationship with the carrier durability and the propagation length, and this is consistent with equation (2-49). As the cross-section of carrier capture increases, the length of propagation will decrease, and thus the durability of the carriers will decrease.

In this part, the density of the interfacial defects was changed from (10^{10}) to (10^{14}) cm^{-2} and the trapping cross-section from (10^{-12} - (10^{-16}) cm^2. The results showed as shown in Figure (4), a decrease in Voc with an increase The cross-section ranges from 0.791 V to 0.776 V, Jsc from 27.69 (mA/cm2) to 20.60 (mA/cm2), F.F from 84.59% to 70.21%, and η from 18.53% to 11.24%, and the reason for this is due to the increase in surface union. For electron-gap pairs, which leads to a decrease in the concentration of carriers as shown in Figure (5a), and we also notice a decrease in quantum efficiency (QE) with an increase in the density of interfacial defects as in Figure (5b).

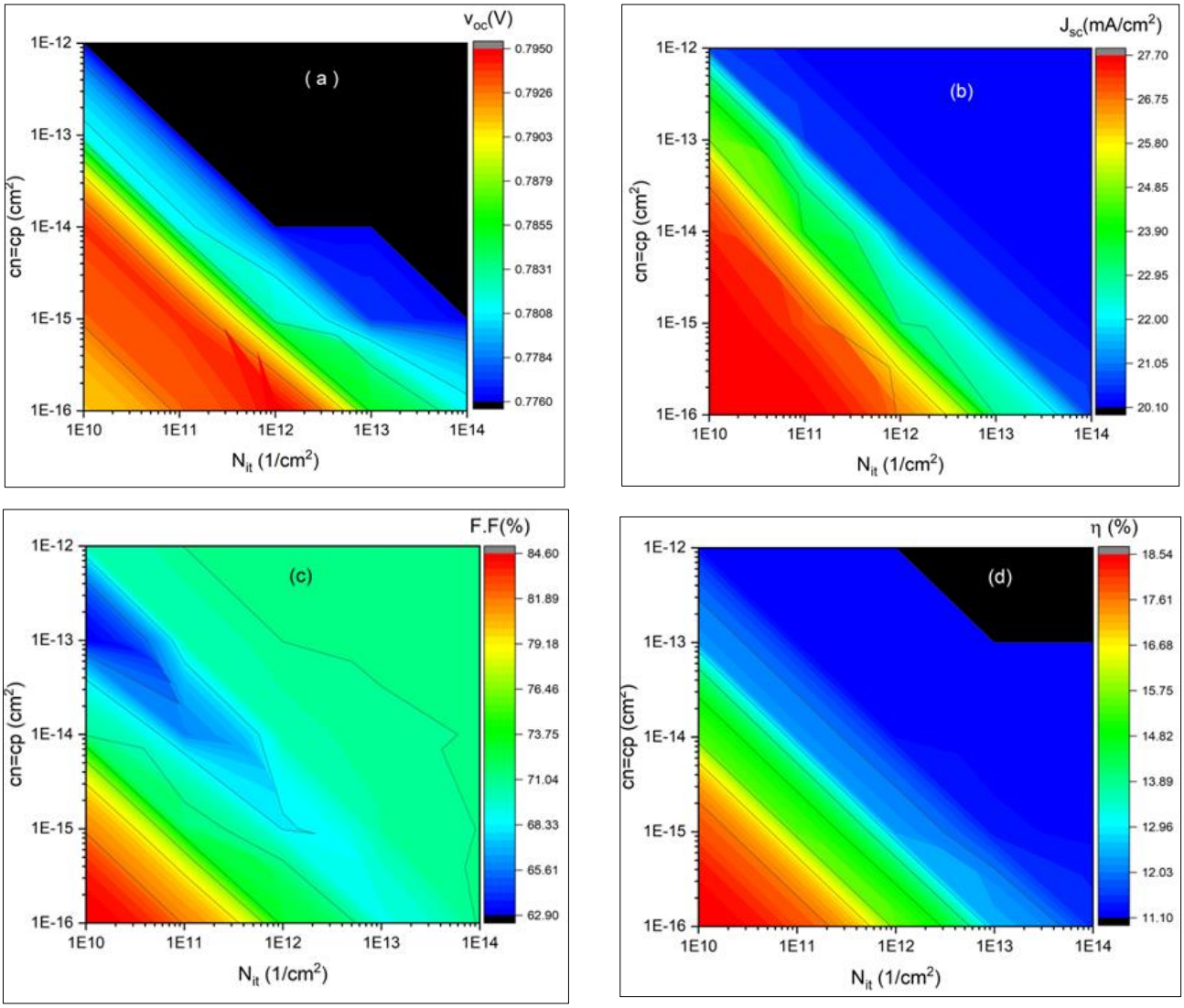

Figure 4 The effect of the trapping cross section and the density of interfacial defects on the operation of the solar cell

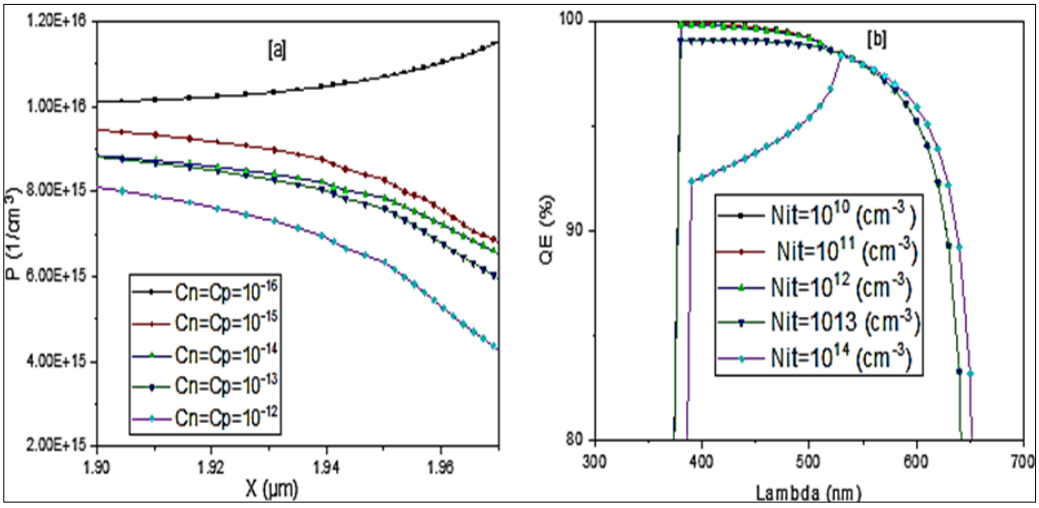

Figure 5 [a] hole current density when changing Cn=Cp [b] Quantum efficiency at each interfacial defect density

5. Conclusion

In this paper, we have studied the Effects of interfacial defects of the p-CuO/n-TiO2 on solar cells using SCAPS-1D. However, these results show a decrease in Voc, Jsc, and η with increasing interfacial defect density The reason for this decrease is due to an increase in the union rate, which leads to a decrease in quantitative efficiency, as in Figure (3).

On the other hand, The carrier capture cross section (Cn, Cp) has a significant impact on the electrical properties of the solar cell because the carrier capture cross section has a relationship with the carrier durability and the propagation length, As the cross-section The results showed as shown in Figure (4), a decrease in Voc, Jsc F.F and η , with an increase The cross-section ranges and the reason for this is due to the increase in surface union. For electron-gap pairs, which leads to a decrease in the concentration of carriers as shown in Figure (5a), and we also notice a decrease in quantum efficiency (QE) with an increase in the density of interfacial defects as in Figure (5b).

Compliance with ethical standards

Disclosure of conflict of interest

No conflict of interest to be disclosed.

References

[1] M. Okil, M. Salem, T. M. Abdolkader, and A. J. S. Shaker, From crystalline to low-cost silicon-based solar cells: A review, vol. 14, no. 5, pp. 1895-1911, 2022.

[2] K. Yoshikawa *et al.*, Silicon heterojunction solar cell with interdigitated back contacts for a photoconversion efficiency over 26%, vol. 2, no. 5, pp. 1-8, 2017.

[3] Y. Zhang and H. J. C. Liu, Nanowires for high-efficiency, low-cost solar photovoltaics, vol. 9, no. 2, p. 87, 2019.

[4] Y. Zhang, Z. Fan, W. Zhang, Q. Ma, Z. Jiang, and D. J. A. A. Ma, High performance hybrid silicon micropillar solar cell based on light trapping characteristics of Cu nanoparticles, vol. 8, no. 5, 2018.

[5] M. S. Salem *et al.*, Physically based analytical model of heavily doped silicon wafers based proposed solar cell microstructure, vol. 8, pp. 138898-138906, 2020.

[6] M. Salem, A. Zekry, A. Shaker, and M. Abouelatta, Design and simulation of proposed low cost solar cell structures based on heavily doped silicon wafers, in *2016 IEEE 43rd Photovoltaic Specialists Conference (PVSC)*, 2016, pp. 2393-2397: IEEE.

[7] M. Rahman, M. Salleh, I. Talib, and M. J. J. o. p. s. Yahaya, Effect of ionic conductivity of a PVC–LiClO4 based solid polymeric electrolyte on the performance of solar cells of ITO/TiO2/PVC–LiClO4/graphite, vol. 133, no. 2, pp. 293-297, 2004.

[8] A. R. Zainun, S. Tomoya, U. M. Noor, M. Rusop, and I. J. M. L. Masaya, New approach for generating Cu2O/TiO2 composite films for solar cell applications, vol. 66, no. 1, pp. 254-256, 2012.

[9] J. Arana, A. P. Alonso, J. D. Rodríguez, J. H. Melián, O. G. Díaz, and J. P. J. A. C. B. E. Peña, Comparative study of MTBE photocatalytic degradation with TiO2 and Cu-TiO2, vol. 78, no. 3-4, pp. 355-363, 2008.

[10] K. Chiang, R. Amal, and T. J. A. i. E. R. Tran, Photocatalytic degradation of cyanide using titanium dioxide modified with copper oxide, vol. 6, no. 4, pp. 471-485, 2002.

[11] H. Irie *et al.*, Visible light-sensitive Cu (II)-grafted TiO2 photocatalysts: activities and X-ray absorption fine structure analyses, vol. 113, no. 24, pp. 10761-10766, 2009.

[12] M. Ichimura and Y. J. M. S. i. S. P. Kato, Fabrication of TiO2/Cu2O heterojunction solar cells by electrophoretic deposition and electrodeposition, vol. 16, no. 6, pp. 1538-1541, 2013.

[13] R. T. J. M. S. Tung and E. R. Reports, Recent advances in Schottky barrier concepts, vol. 35, no. 1-3, pp. 1-138, 2001.

[14] S. Hussain *et al.*, Cu2O/TiO2 nanoporous thin-film heterojunctions: Fabrication and electrical characterization, vol. 25, pp. 181-185, 2014.

[15] S. Hussain *et al.*, Fabrication and photovoltaic characteristics of Cu2O/TiO2 thin film heterojunction solar cell, vol. 522, pp. 430-434, 2012.

[16] Y. H. Khattak *et al.*, Effect of CZTSe BSF and minority carrier life time on the efficiency enhancement of CZTS kesterite solar cell, vol. 18, no. 6, pp. 633-641, 2018.

[17] F. A. Jhuma, M. Z. Shaily, M. J. J. M. f. R. Rashid, and S. Energy, Towards high-efficiency CZTS solar cell through buffer layer optimization, vol. 8, pp. 1-7, 2019.

[18] F. H. Oraibi and F. A. J. J. o. K.-P. AL-Tememe, Theoretical Study of the effect of impurity concentrations on the efficiency of the single crystal silicon solar cell, vol. 4, no. 1, 2012.

[19] H. Guo, Y. Li, X. Guo, N. Yuan, and J. J. P. B. C. M. Ding, Effect of silicon doping on electrical and optical properties of stoichiometric Cu2ZnSnS4 solar cells, vol. 531, pp. 9-15, 2018.

[20] K. Mukhopadhyay, P. F. H. Inbaraj, and J. J. J. M. R. I. Prince, Thickness optimization of CdS/ZnO hybrid buffer layer in CZTSe thin film solar cells using SCAPS simulation program, 2018.

[21] F. Baig, Numerical analysis for efficiency enhancement of thin film solar cells, Universitat Politècnica de València, 2019.

[22] A. Spies, J. Reinhardt, M. List, B. Zimmermann, and U. J. E. P. i. O. P. Würfel, Impact of charge carrier mobility and electrode selectivity on the performance of organic solar cells, pp. 401-418, 2017.

[23] F. Baig *et al.*, Numerical analysis of a novel FTO/n-MAPbI3/p-MAPbI3/p-MAPbBr3 organic–inorganic lead halide perovskite solar cell, vol. 13, no. 9, pp. 1320-1327, 2018.